Microfluidic Crystals: Dynamic Interplay between Rearrangement Waves and Flow

Jan-Paul Raven and Philippe Marmottant*

Laboratoire de Spectrométrie Physique, B.P. 87, F-38402 St. Martin d'Hères Cedex, France†

(Received 3 September 2008; published 26 February 2009)

Microfluidic crystals are assemblies of miniature bubbles or drops flowing in channels. We explore here the flow of these crystals, when submitted to a given driving pressure. The flow velocity is linked to the finite number of elements in the channel width, and presents discontinuities when the crystal structure changes. At the transition from one structure to the other original dynamic features appear. The flow can self-regulate itself on a fixed velocity whatever the driving pressure, or, on the contrary, can spontaneously pulsate. All these features are predicted by simply considering the crystal's energy and friction, and looking at the propagation of structure rearrangements. We anticipate these results to improve the control over the structure of dense two-phase flows in microfluidic systems.

DOI: 10.1103/PhysRevLett.102.084501 PACS numbers: 47.55.db, 47.60.−i, 83.50.Ha, 83.80.Iz

Recently, several microfluidic methods have been developed to generate miniature bubbles or droplets. These methods are usually based on channels, micrometric in size, with specific geometries to assemble two fluid phases [1–3]. At small scales flows are laminar, and induce extremely well controlled bubble or droplet sizes [2]: standard deviation in size can be as little as 0.1% [4].

Since bubbles or droplets have identical sizes, they spontaneously self-assemble in ordered lattices that are called *microfluidic crystals* [5–11]. A surfactant solution prevents coalescence. By including a hardening step these assemblies could become the basis of new solid metamaterials [6,12], with applications in acoustics as phononic crystals, photonics, filtration, and other technologies needing a precisely ordered material. Furthermore, creating foams and emulsions is of interest within a lab-on-a-chip. Indeed bubbles, and similarly droplets, can be seen as volume samples, typically of one picoliter [13], that are manipulated and analyzed within a miniature lab [14].

Microfluidic crystals are highly confined in channels, whose size is comparable to the element size. Their discrete (noncontinuous) composition in individual elements leads to original features. For this field, integrating foams in microfluidics, the term ''discrete microfluidics'' was recently suggested [15].

Here we show that their flow presents rich nonlinear dynamics, because of their discrete composition. Indeed their rate of flow is far from being proportional (linear) to the driving pressure. Because of changes in the crystalline pattern, the flow can (i) self-regulate and lock to a fixed velocity, whatever the pressure, or on the reverse (ii) periodically pulsate at a given pressure. We will present experiments describing the first case. We will provide key elements to the understanding of this dynamics, namely, the drag of different crystalline patterns, and the presence of pattern rearrangements that can propagate. These new elements will also help with the understanding of the second case, with oscillations observed experimentally [9,16], but whose conditions of apparition were unclear.

To investigate the flow of these microfluidic crystals, we built a microfluidic bubble generator. The device we use for microbubble generation and observation is based on a flow-focusing geometry [1,2], and consists in a planar network of $h = 100\ \mu$m height rectangular ducts produced by soft-lithography [17]. Bubble production [2,4,11] is controlled by two parameters: the gas pressure P_g that inflates bubbles and thereby pushes the structure in the channels, and the liquid flow rate Q_l that segments the gas jet and creates soapy liquid films between and around bubbles [see Fig. 1(a)].

Various crystalline patterns appear when tuning up the gas pressure: bubble volume V_b increases [2], and the flow transits from bubbly to a foam flow, with a structure that contains fewer and fewer bubble rows [11] in a channel. Simple foam hexagonal structures are characterized by the number of bubble rows in the channel width: hex-one, hex-two, hex-three, and so on [9]. From now on, we will focus on hex-one and hex-two structures that are easily de-

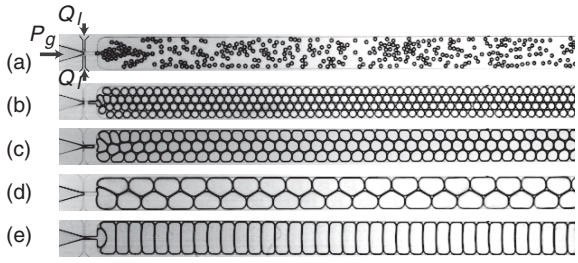

FIG. 1. Microfluidic crystals bubbles are generated one by one in the inlet of the microchannel, injecting simultaneously gas with a driving pressure P_g, and liquid of flow rate Q_l. (a) At small bubble sizes, we obtain a bubbly flow. (b)–(e) By increasing gradually the gas pressure from 1 to 10 kPa (with a liquid flow rate of the order of a few μl/min) the bubble size grows and flowing microfluidic crystals self-assemble. The number or rows in the width ($w = 1$ mm) decreases by steps. The hexagonal structure is named according to the number of rows: hex-four (b), hex-three (c), hex-two (d), hex-one (e).

scribed, but the present results can be extrapolated to higher number crystals [18]. In Fig. 2(a), we plot the flow velocity versus the imposed gas pressure, for a narrow channel. At low pressures small bubbles self-assemble in the hex-two structure, while at high pressures larger bubbles organize in hex-one structure.

In between these homogeneous structures, transition regions exist that present original features. We will see three different kinds of transitions depending on Q_l: we start here with the one observed at medium Q_l, because it will shed light on all the others. We observe a remarkable behavior in this transition region: the flow velocity plateaus at a constant value for a large range of driving pressure. Since the flow rate is stable in time and against pressure variation we obtain a *self-regulated* flow. As a side effect, the bubble volume also stays constant, because it is proportional to the velocity [11]. The hex-one structure changes continuously in a hex-two structure at a front whose position is *stationary*, see movie 1 in Ref. [19]. This position depends only on the gas pressure: it is located further downstream at higher P_g, increasing the hex-one proportion. The analogy with a first order phase transition is striking. A liquid-vapor isotherm presents a similar plateau in the pressure vs density diagram, and hysteresis at transitions.

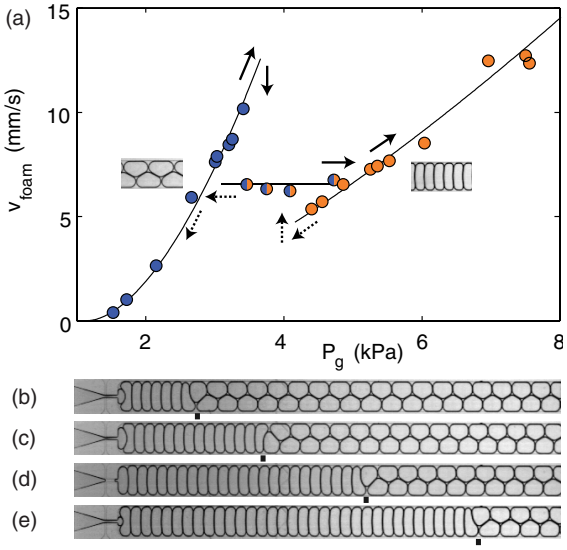

FIG. 2 (color online). Transition from one flowing crystal to the other, with a steady coexistence because of a stationary rearrangement wave. (a) Flow velocity as a function of the applied gas pressure P_g (at $Q_l = 5\ \mu\mathrm{l/min}$). For increasing P_g the structure is the following: hex-two (image insert), then a coexistence of hex-one and hex-two [labels (b)–(e) indicate the image below], then hex-one (image insert). Continuous arrows indicate the path for growing P_g, dashed arrows for decreasing P_g. (b)–(e) The plateau in velocity corresponds to a *self-regulated* situation where a structure transforms continuously into the other at a *stationary front* indicated by a vertical bar. Snapshots are taken for pressure P_g 3.46 kPa (b), 3.75 kPa (c), 4.09 kPa (d), 4.73 kPa (e); see movie 1 in Ref. [19].

The structure transformation involves topological rearrangements known as T1 changes. These events correspond to an exchange in neighbor [Figs. 3(a)–3(g)] that decreases the energy associated with the liquid-gas interfaces [20]. We will call the sequence of T1 events at the interface between structures a "T1 wave." Actually, in the reference frame of the foam, this T1 wave propagates upstream. Further on we will show that the equilibration of the foam velocity v_{foam} to the upstream T1-wave velocity v_{T1} sets the position of the front. The plateau value in velocity has therefore the value $v_{\mathrm{foam}} = -v_{\mathrm{T1}}$.

Studying T1 events in foams is currently a lively research topic, as they are the basic element of plasticity in amorphous materials [7,21–23]. A recent publication of Durand *et al.* [24] showed that the typical relaxation time after a T1 event is related to the viscoelastic properties of the gas-liquid interface, notably the surface shear plus elongational viscosity $\mu_s + \kappa$ and the Gibbs elasticity ϵ. Their analysis gives a characteristic time:

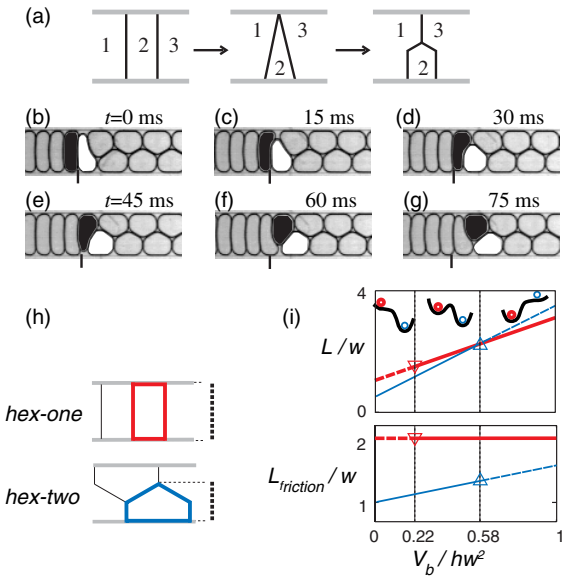

FIG. 3 (color online). Time-resolved dynamics of rearrangements at the front between structures. (a) Schematic representation of a T1 rearrangement (neighbor swapping) next to the upper wall. (b)–(g) Time series at the interface between the two structures [close-up of Fig. 2(b)]. The junction between these structures leads to a mismatch with a deformed bubble (indicated in white), which triggers a T1 next to the upper wall. (e)–(f) The next bubble (in black) is now deformed and will on its turn experience a T1 next to the lower wall. (h) Drawing containing the perimeter L, proportional to bubble energy, and friction length L_{fric}. (i) Predicted energy L and friction L_{fric} as a function of bubble volume for the two structures (thick: hex-one, thin: hex-two). Lines: stable state; dashes: unstable state; triangles: experimental limits of stability. Sketches illustrate the stability with an energy potential, the thick "wheel" stands for the hex-one state while the thin "wheel" stands for the hex-two state. Coexistence of the two structures is possible only in the region between the vertical dotted lines, hex-one being metastable and hex-two stable.

$\tau_{T1} = (\mu_s + \kappa)/\epsilon \approx 30$ ms for a solution of SDS, a typical surfactant. We predict the typical speed to be

$$v_{T1} = \frac{\Delta x}{\tau_{T1}}, \tag{1}$$

with $\Delta x = V_b/hw$ the distance between two bubbles in the hex-one structure. It gives a value of 12 mm/s which is the same order of magnitude as the measured speed $v_{foam} = 7$ mm/s, seeming to confirm that surface viscosity is the main dissipation mechanism. An alternative model where T1 speed is related to friction on the wall would give a much smaller and unrealistic relaxation time.

A drop in interfacial energy is a necessary, but not sufficient, condition for a topological rearrangement to occur. The energy for one bubble is just the surface tension γ times the total bubble surface (gas-liquid interface). Here we consider bubbles of constant volume, and the only variable part of energy is $E = \gamma hL$, with L the perimeter seen on images. Thus it is convenient and graphical to simply compare the apparent bubble perimeter L for the hex-one and hex-two structure [Fig. 3(h)]. It can be calculated analytically (see also [25]), assuming perfectly dry foams in local equilibrium, for the two different structures: $L^{\text{hex-one}} = (1 + 2V_b/hw^2)w$, $L^{\text{hex-two}} = [1/2 + (2 + \sqrt{3}/2)V_b/hw^2]w$. As can be seen in Fig. 3(i), these equations imply a crossover in energy at $V_c/hw^2 = \sqrt{3}/3 \simeq 0.58$, for which $L^{\text{hex-one}} = L^{\text{hex-two}}$.

For the foam undergoing a T1 wave, the hex-two structure has the lowest energy (the bubble volume $V_b/hw^2 = 0.36$ is lower than V_c). The hex-two structure is said to be a stable state while the hex-one structure is a metastable state. By shape deformations a bubble can explore the energy landscape. Each structure is (linearly) stable against small amplitude deformations, being at the local minimum of an energy potential, see the sketch in the middle of Fig. 3(i). The T1 wave causes a large deformation of the bubble shape and is therefore the large amplitude (nonlinear) route to pass the energy barrier between the metastable state and the stable state [26].

This coexistence of structure is in fact limited to an intermediate range of bubble volumes. Indeed, if the bubble volume is too low (for hex-one) or too large (for hex-two) one structure becomes linearly unstable just after formation. These critical volumes, measured on experiments, are indicated on Fig. 3(i) by two vertical lines, and define the extent of the coexistence zone.

We now expose simple arguments based on the different friction of structures, to explain the self-regulating mechanism of the front. The structure present in the channel influences the total flow resistance R, a quantity that relates the velocity to the imposed pressure:

$$P_g = R v_{foam}^{\alpha}, \tag{2}$$

with α a coefficient in between 1/2 and 2/3 [27–31]. With a coexistence of structures the resistance writes

$$R \sim \phi n R_{friction}^{\text{hex-one}} + (1 - \phi) n R_{friction}^{\text{hex-two}}, \tag{3}$$

where we have introduced n the total number of bubbles, $\phi = n^{\text{hex-one}}/n$ the proportion of hex-one bubbles, and $R_{friction}$ the friction per bubble. Cantat *et al.* demonstrated a geometrical relation between $R_{friction}$ and the foam structure [28]: $R_{friction} \propto L_{friction}$, with $L_{friction}$ the projection of L in the direction normal to the flow [Fig. 3(i)]. It results from the local friction due to motion of the liquid that is largely confined to the menisci in between bubbles and the channel walls. This friction contact area corresponds approximately to the black part on the images. Since the channel is very thin, dissipative friction occurs mainly on the (transparent) walls that are in front of and behind the bubbles, along the axis of view. The calculation of $L_{friction}$ gives [32]: $L_{friction}^{\text{hex-one}} = 2w$ and $L_{friction}^{\text{hex-two}} = [1 + (1/\sqrt{3})V_b/hw^2]w$. The hex-one bubbles always have a higher resistance to flow than the hex-two bubbles; see Figs. 3(h) and 3(i): their transverse span is larger. A similar result can be obtained for higher order crystals (hex-two compared with hex-three, and so on), with less pronounced effects [18] because of smaller friction differences.

The difference in the friction of structures provides a feedback to regulate the position of the front. For instance, a slight displacement of the front downstream will increase ϕ and the total drag by Eq. (3), thereby slowing down the foam. This will redirect the interface towards its initial position. The fraction ϕ of hex-one bubbles, and thus the equilibrium position of the front, is given by Eq. (2) and (3) using $v_{foam} = -v_{T1}$. A change in P_g is compensated by a resistance change and by a linear variation of the front position along the channel.

There are two other original flows intermediate between hex-one and hex-two structures, that appear when tuning the second control parameter, the liquid flow rate. The self-regulated regime ranges in an intermediate domain (see phase diagram in [19]). For higher liquid flow rates, the flow is unstable, with transient appearances of the hex-two structure that are advected out of the channel. For lower liquid flow rates, the flow spontaneously pulsates, oscillating periodically between the production of each structure [32].

These regimes have the same bubble volumes but correspond to different foam flow speeds. Indeed when Q_l is increased, it is necessary to tune up simultaneously P_g to maintain the *same* bubble volume [2,11], which leads to an increase of the gas flow and foam speed v_{foam}.

We can now propose a general classification of the transition regimes, from the comparison of the foam speed with the T1-wave velocity, using the language of large amplitude nonlinear instabilities (see Fig. 4):

(a) The structure coexistence for which $v_{foam} = -v_{T1}$ corresponds to a stationary instability of the hex-one–hex-two interface.

(b) The large flow velocity case with $v_{foam} > -v_{T1}$ can be described as an advected instability.

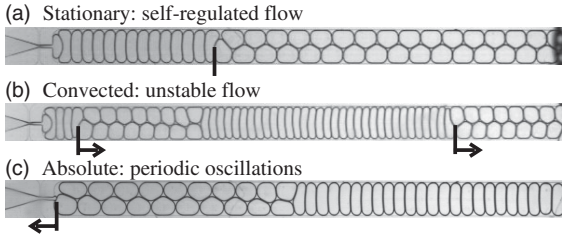

FIG. 4. Ordering of the complex flow structures. Arrows indicate the absolute velocity of the rearrangement front. See [19] for movies. (a) $Q_l = 5\ \mu\mathrm{l/min}$, $P_g = 3.8$ kPa; (b) $Q_l = 10\ \mu\mathrm{l/min}$, $P_g = 9.3$ kPa; (c) $Q_l = 4\ \mu\mathrm{l/min}$, $P_g = 2.9$ kPa.

(c) The low velocity case with $v_{\mathrm{foam}} < -v_{\mathrm{T1}}$ leading to a periodically oscillating flow [32], is now interpreted as an absolute instability. Rapidly after its nucleation, a T1 wave reaches the orifice thereby leading to hex-two formation at the orifice, until bubble volumes are too large, which triggers the periodic oscillation.

The first stationary case is marginal for systems with an imposed *flow rate* [33]. Here the *pressure* is imposed, and the self-adaptation of the flow rate remarkably produces a stationary domain with a finite extent.

The dynamic interplay between structure and flow is therefore ruled by the velocity of propagation of structure rearrangements. The complex flow that we describe here is an interesting example of dynamic self-organization, that is rich in behavior and can be understood with simple physical arguments. On the technological level, it opens new possibilities for the generation of controlled bubble or droplet samples. The oscillating regime offers a route to the production of bubble samples with a known polydispersity. The locking of the bubble size to a particular value in the structure coexistence domain permits very robust bubble generation. Small fluctuations in the inlet pressure do not lead to a variation in bubble size but are absorbed by a small shift in the hex-one–hex-two interface position. In its turn, the avalanche of T1 changes at this interface allows for a, to our best knowledge, uniquely easy way to study this key element in amorphous material science: the T1 changes are stationary in space and their number is in principle unlimited in time.

We would like to acknowledge fruitful discussion with François Graner, Wiebke Drenckhan, and Simon Cox.

*philippe.marmottant@ujf-grenoble.fr
†CNRS-UMR 5588, Université Grenoble I, Grenoble, France.

[1] S. L. Anna, N. Bontoux, and H. A. Stone, Appl. Phys. Lett. **82**, 364 (2003).
[2] P. Garstecki, I. Gitlin, W. DiLuzio, G. M. Whitesides, E. Kumacheva, and H. A. Stone, Appl. Phys. Lett. **85**, 2649 (2004).
[3] G. F. Christopher and S. L. Anna, J. Phys. D **40**, R319 (2007).
[4] B. Dollet, W. van Hoeve, J.-P. Raven, P. Marmottant, and M. Versluis, Phys. Rev. Lett. **100**, 034504 (2008).
[5] T. Thorsen, R. W. Roberts, F. H. Arnold, and S. R. Quake, Phys. Rev. Lett. **86**, 4163 (2001).
[6] M. Minseok, Z. Nie, S. Xu, P. C. Lewis, and E. Kumacheva, Langmuir **21**, 4773 (2005).
[7] W. Drenckhan, S. J. Cox, H. Holste, D. Weaire, and N. Kern, Colloids Surf. A **263**, 52 (2005).
[8] T. Beatus, T. Tlusty, and R. Bar-Ziv, Nature Phys. **2**, 743 (2006).
[9] P. Garstecki and G. M. Whitesides, Phys. Rev. Lett. **97**, 024503 (2006).
[10] A. van der Net, G. W. Delaney, W. Drenckhan, D. Weaire, and S. Hutzler, Colloids Surf. A **309**, 117 (2007).
[11] J.-P. Raven, P. Marmottant, and F. Graner, Eur. Phys. J. B **51**, 137 (2006).
[12] G. M. Whitesides and M. Boncheva, Proc. Natl. Acad. Sci. U.S.A. **99**, 4769 (2002).
[13] T. M. Squires and S. R. Quake, Rev. Mod. Phys. **77**, 977 (2005).
[14] G. M. Whitesides, Nature (London) **442**, 368 (2006).
[15] W. Drenckhan, S. Cox, G. Delaney, H. Holste, D. Weaire, and N. Kern, Colloids Surf. A **263**, 52 (2005).
[16] J.-P. Raven and P. Marmottant, Phys. Rev. Lett. **97**, 154501 (2006).
[17] D. Duffy, J. McDonald, O. Schueller, and G. Whitesides, Anal. Chem. **70**, 4974 (1998).
[18] J. P. Raven, Ph.D. thesis, Université Joseph Fourier (Grenoble I), 2007, http://tel.archives-ouvertes.fr/tel-00192819/.
[19] See EPAPS Document No. E-PRLTAO-102-024911 for movies of transitions between flowing microfluidic crystals. For more information on EPAPS, see http://www.aip.org/pubservs/epaps.html.
[20] D. Weaire and S. Hutzler, *The Physics of Foams* (Oxford University Press, Oxford, 1999).
[21] J. Lauridsen, M. Twardos, and M. Dennin, Phys. Rev. Lett. **89**, 098303 (2002).
[22] I. Cantat and O. Pitois, Phys. Fluids **18**, 083302 (2006).
[23] B. Dollet and F. Graner, J. Fluid Mech. **585**, 181 (2007).
[24] M. Durand and H. A. Stone, Phys. Rev. Lett. **97**, 226101 (2006).
[25] P. Garstecki and G. M. Whitesides, Phys. Rev. E **73**, 031603 (2006); URL http://link.aps.org/abstract/PRE/v73/e031603.
[26] A visual analogy is the propagation of the fall in a line of dominoes, each starting from a vertical (metastable) state and ending in a fallen (stable) state.
[27] F. P. Bretherton, J. Fluid Mech. **10**, 166 (1961).
[28] I. Cantat, N. Kern, and R. Delannay, Europhys. Lett. **65**, 726 (2004).
[29] E. Terriac, J. Etrillard, and I. Cantat, Europhys. Lett. **74**, 909 (2006).
[30] N. D. Denkov, V. Subramanian, D. Gurovich, and A. Lips, Colloids Surf. A **263**, 129 (2005).
[31] N. D. Denkov, S. Tcholakova, K. Golemanov, and V. S. A. Lips, Colloids Surf. A **282–283**, 329 (2006).
[32] J.-P. Raven and P. Marmottant, Phys. Rev. Lett. **97**, 154501 (2006).
[33] J. M. Chomaz, Phys. Rev. Lett. **69**, 1931 (1992).